International Journal of Heat and Fluid Flow 30 (2009) 854–867

Contents lists available at ScienceDirect

International Journal of Heat and Fluid Flow

journal homepage: www.elsevier.com/locate/ijhff

Two-phase flow instabilities in a silicon microchannels heat sink

D. Bogojevic[a], K. Sefiane[a,*], A.J. Walton[b], H. Lin[b], G. Cummins[b]

[a] School of Engineering, University of Edinburgh, Mayfield Road, King's Buildings, EH9 3JL Edinburgh, UK
[b] Scottish Microelectronic Centre, Joint Research Institute for Integrated Systems, School of Engineering, The University of Edinburgh, EH9 3JF, UK

ARTICLE INFO

Article history:
Received 30 November 2008
Received in revised form 25 March 2009
Accepted 26 March 2009
Available online 1 May 2009

Keywords:
Microchannels
Two-phase flow boiling
Instability
Silicon heat sinks
Microsensors

ABSTRACT

Two-phase flow instabilities are highly undesirable in microchannels-based heat sinks as they can lead to temperature oscillations with high amplitudes, premature critical heat flux and mechanical vibrations. This work is an experimental study of boiling instabilities in a microchannel silicon heat sink with 40 parallel rectangular microchannels, having a length of 15 mm and a hydraulic diameter of 194 μm. A series of experiments have been carried out to investigate pressure and temperature oscillations during the flow boiling instabilities under uniform heating, using water as a cooling liquid. Thin nickel film thermometers, integrated on the back side of a heat sink with microchannels, were used in order to obtain a better insight related to temperature fluctuations caused by two-phase flow instabilities. Flow regime maps are presented for two inlet water temperatures, showing stable and unstable flow regimes. It was observed that boiling leads to asymmetrical flow distribution within microchannels that result in high temperature non-uniformity and the simultaneously existence of different flow regimes along the transverse direction. Two types of two-phase flow instabilities with appreciable pressure and temperature fluctuations were observed, that depended on the heat to mass flux ratio and inlet water temperature. These were high amplitude/low frequency and low amplitude/high frequency instabilities. High speed camera imaging, performed simultaneously with pressure and temperature measurements, showed that inlet/outlet pressure and the temperature fluctuations existed due to alternation between liquid/two-phase/vapour flows. It was also determined that the inlet water subcooling condition affects the magnitudes of the temperature oscillations in two-phase flow instabilities and flow distribution within the microchannels.

1. Introduction

Flow boiling in microchannels has attracted attention as a potential technology for high heat flux dissipation. The main advantage of such technology is the possibility of achieving high heat transfer coefficients using low coolant flow rates that require a low pressure drop and consequently reduced pumping power requirements (Lin et al., 2002). However, the main disadvantages of this approach to cooling are flow instabilities and back flow reversals, which occur under certain flow boiling conditions. These instabilities with characteristic pressure drop and flow rate oscillation are undesirable, as they can lead to high amplitude temperature oscillations with premature critical heat flux (CHF) and mechanical vibrations. These vibrations, together with the thermal stress set up in the heat exchanger material, can cause heat exchanger burn-out and mechanical breakdown. Two-phase flow instabilities in minichannels and microchannels are more intense than in conventional channels due to the low flow velocities and the confined space available for bubbles growth. These instabilities result in a lower CHF than would be obtained with stable flow in the microchannels based heat sink (Bergles and Kandlikar, 2005). Instabilities in microchannels have been reported by many authors, but in many cases with different oscillation amplitude and frequency under similar mass and heat flux conditions. One possible reason for this was proposed by Wang et al. (2008) who suggested that the configuration of inlet and outlet regions can significantly influence the type of instabilities observed.

Qu and Mudawar (2003) have investigated flow boiling of water in a heat sink containing 21 copper parallel microchannels. They reported severe pressure drop oscillations caused by interaction between the vapour generated within the channels and the compressible volume of the inlet manifold. The authors found that a throttling valve installed immediately upstream of the heat sink significantly reduced these instabilities. Zhang et al. (2005) have used doped silicon sensors to measure transient pressure fluctuations frequencies during boiling in a single microchannel with water as the working fluid. The authors observed frequencies ranging from 3 to 40 Hz, and recorded up to 138 kPa transient pressure fluctuations due to bubble nucleation. Explosive generation of vapour and the temporal behaviour of temperature and pressure in parallel triangular microchannels have been observed by Hetsroni

* Corresponding author. Tel.: +44 131 6504873; fax: +44 131 6506551.
E-mail address: k.sefiane@ed.ac.uk (K. Sefiane).

0142-727X/$ - see front matter © 2009 Elsevier Inc. All rights reserved.
doi:10.1016/j.ijheatfluidflow.2009.03.013

Nomenclature

A	area of the heated microchannels region, m^2
c_p	specific heat capacity, J/g K
f	frequency, Hz
G	mass flux, kg/m^2 s
I	current, A
m	mass flow rate, g/s
P	pressure, bar
Q	total power, W
q	heat flux, kW/m^2
R	resistance, Ω
T	temperature, °C
t	time, s
V	voltage, V

Greek symbols

ΔP	pressure drop, bar
φ	portion of the total power transferred to the water

Subscripts

in	inlet
out	outlet

et al. (2002, 2003, 2005, 2006). They found that the amplitude of pressure drop fluctuations increased with increasing heat flux and vapour quality at constant values of mass flux.

Wu and Cheng (2003a, 2003b, 2004) reported two oscillatory flow boiling modes in microchannels depending on the heat to mass flux ratio. It was found that mass flux and pressure oscillated out of phase in these two boiling modes, and the large amplitude oscillations of pressure and temperature could be self-sustained. Wang et al. (2007) experimentally investigated dynamic instabilities of flow boiling of water in parallel microchannels as well as in a single microchannel. The authors classified these instabilities into stable and unstable regimes, depending on the heat to mass flux ratio. Two types of unstable oscillations were reported, one with long-period oscillations and another with short-period oscillations in temperature and pressure.

Kandlikar et al. (2006) have assessed the effects of an inlet pressure restrictor and fabricated nucleation sites as a means of stabilizing the two-phase flow instabilities in microchannels. The authors found that fabricated nucleation sites in conjunction with the pressure restrictor having a flow area of 4% of the channel cross-sectional area completely eliminated the instabilities associated with the reverse flow. Kosar et al. (2006) have experimentally investigated the effects of inlet orifices with various geometries on the suppression of flow boiling instabilities in parallel microchannels. They have shown that for sufficiently high inlet pressure restriction imposed by the inlet orifices, parallel channels and upstream compressible volume instabilities are eliminated. Kuo and Peles (2009) experimentally studied the effects of pressure on flow boiling instabilities in microchannels. They found that high system pressure moderates instabilities by reducing the void fraction, the superheat needed to activate bubble nucleation and bubble departure diameter. Local transient temperature measurements showed lower magnitudes and higher frequencies of oscillations at high system pressure.

The aim of the present experimental study is to investigate two-phase flow instabilities inside a uniformly heated silicon heat sink consisting of 40 parallel rectangular microchannels with hydraulic diameters of 194 μm, using water as cooling liquid. Two standard pressure transducers and thin nickel film thermometers integrated on the back side of the silicon chip were used together with simultaneous visualisation to examine of oscillation frequencies for different flow boiling modes. The effects of inlet water temperature on flow boiling instabilities were experimentally studied, with the influence of different subcooling conditions on the magnitude of temperatures as well as the influence on the flow distribution within channels being assessed. Using a larger number of microchannels entails the risk of a non-uniform distribution during the flow boiling in the microchannels. One of the objectives of this study is to investigate the effect of non-uniform distribution within the channels on both flow instabilities and the temperature distribution. It is much more likely that in real cooling applications (e.g. cooling of CPU's) heat sinks with a large number of channels will be used (to cover an area $>10 \times 10\ mm^2$) rather than heat sinks with just a few channels. With the main issues related to using flow boiling as potential cooling technology being flow instabilities and non-uniform distribution are thoroughly investigated and discussed.

2. Experimental setup and procedure

2.1. Experimental facility and procedure

The experimental setup consists of a boiling flow loop and test module (Fig. 1). The flow loop was designed to deliver deionised and degassed water from a reservoir into the test module with microchannels at constant flow rate using a variable speed gear pump. A 15 μm filter was used to prevent any solid particles from entering the test section. Flow rates were measured by a thermal mass flow meter calibrated for the range from 1 to 50 g/min based on water. Subcooling conditions for water (test module inlet temperature) were maintained using an electrical pre-heater with a PID controller. The flow rate through the test module was determined by adjusting the bypass valve and a fine needle valve located upstream of the test module. Vapour generated in the test module returned to the reservoir where it condensed and the water reservoir-condensing chamber was kept under atmospheric pressure during the experiments.

The test module was a silicon heat sink with 40 parallel rectangular channels, 15 mm long, 273 μm deep, 150 μm wide spaced by 100 μm. The microchannels with integrated inlet and outlet manifolds were etched into a silicon wafer using the deep reactive ion etching process. A lift-off process was used to form temperature sensors on the back side of the wafers, after which a 500 μm thick Pyrex glass cover plate was anodically bonded to the silicon wafer to seal and enable visualisation of boiling within the microchannels. On the back side of the device there are five integrated sensors made from a thin nickel film for temperature measurements and an aluminium heater track for uniform heating of the microchannels area. The sensors were integrated between the heater and the microchannels, and were located 112 μm underneath the bottom of the channels. Fig. 2a shows the layout of masks used for the microfabrication process, while the layout of a single sensor is shown in Fig. 2b. The location of the sensors $T1$–$T5$ enables the measurement of temperatures in both the flow stream direction and the transverse direction. Most authors investigating flow boiling instabilities have used temperature sensors located only along the direction of the flow stream. Water is supplied through

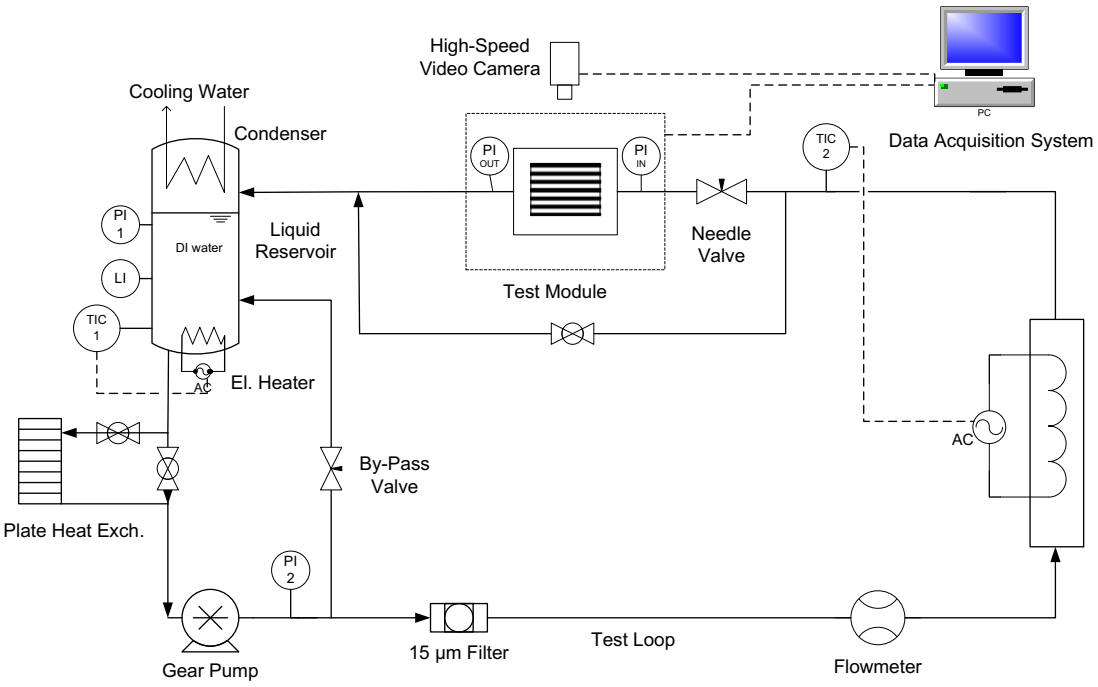

Fig. 1. Scheme of the experimental setup.

external stainless tubes, connected to the inlet/outlet holes drilled in the Pyrex glass cover plate. Two small o-rings are used to seal the connections and prevent any leaks from the heat sink. Electrical connections for the heater and the sensors are made via aluminium pads deposited on the backside of the device and spring probes connected to the measurement instrumentation. The silicon heat sink is placed in a sandwich between the top and the bottom frames as shown in Fig. 3a. The bottom frame is made from PEEK plastic which has good thermal insulation property while the top frame is a transparent polycarbonate plastic with holes machined for external tubes and a square window for visualisation inside microchannels (Fig. 3b).

Prior to carrying out the experiment, deionised water in the reservoir is degassed by vigorous boiling in the reservoir for approximately one hour. Afterwards, the flow rate and the inlet water temperature is adjusted to the desired values. Flow boiling conditions inside the microchannels were then set by either increasing the heat flux with constant flow rate or decreasing the flow rate with constant heat flux.

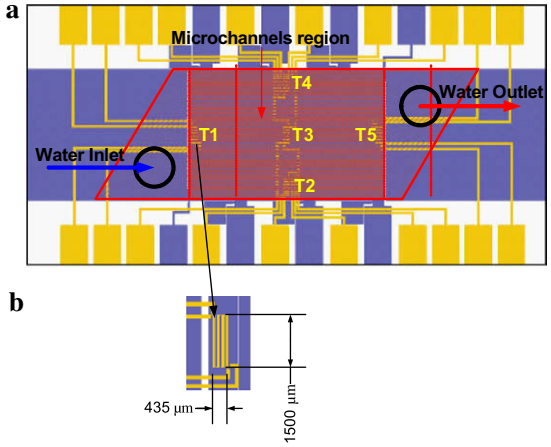

Fig. 2. Layout of (a) masks for the channels, the heater and the sensors and (b) a single temperature sensor.

2.2. Data acquisition system and measurements uncertainty

The heat flux transferred to the water was calculated from $q = \varphi VI/A$, where V and I are the input voltage and the current across the film heater, A the area of the heated microchannels region, and φ the portion of the total power transferred to the water. In order to determinate φ, a series of single-phase heat transfer experiments were carried out prior to boiling experiments. The portion of the total power transferred to the water was computed from $Q = mc_p(T_{out} - T_{in})$, where the specific heat capacity was calculated based on the mean water temperature (average of the water inlet and outlet temperatures). The total power to the heater was determined from product of the voltage (V) and current (I) with φ being computed from $\varphi = Q/VI$. The values of φ were found to be in the range of 0.83–0.95 depending on the heat flux and flow rate. The mean value of 0.89 was used to determine the heat flux transferred to the water. It is worth noting that the procedure of calculating the portion of the total power transferred to the water was similar to that used by Hetsroni et al. (2005), Liu et al. (2005) and Wang et al. (2007).

Pressure, temperature and voltage from the microsensors were acquired and recorded using a 16-bit NI SCXI 1600 data acquisition system from National Instruments and a LabView software interface. Two absolute pressure transducers and two T-type thermocouples, located immediately upstream and downstream of the test module were also used for monitoring the inlet/outlet pressures and temperatures respectively. The pressure transducers used (Omega PXM219 series) have a full scale accuracy of 0.25% (2.5 bar) and a response time of 2 ms. The standard accuracy of the thermal mass flow meter (Bronkhorst L30 Series) was ±0.5 g/min. The uncertainties related to thermocouples measurements were ±0.5 °C for T-type thermocouples.

The use of microfabrication techniques enables more accurate and reproducible channel dimensions. In the x–y plane the dimensions and layout of the channels are largely determined by the

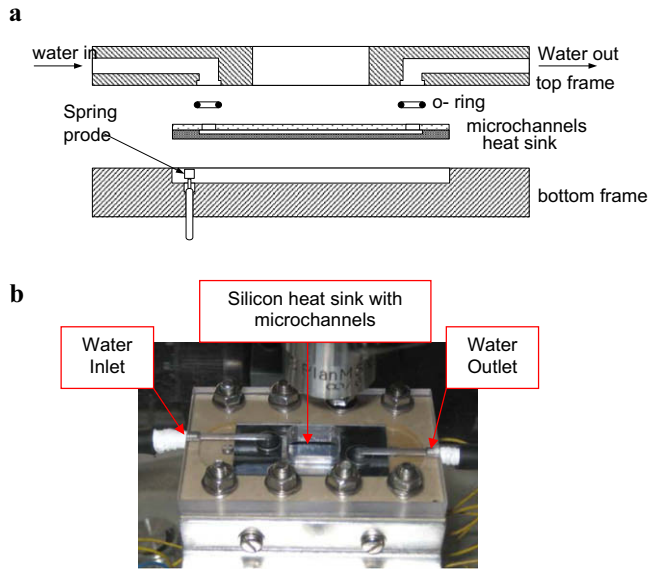

Fig. 3. (a) Test module construction and (b) picture of the test module.

mask pattern. The mask pattern is transferred onto the silicon using photolithography and the pitch of the channels is always faithfully reproduced. The width of the channel depends upon both the lithography and etch process biases. The variations of channel width were considerably less than the accuracy of the Vickers CSS microscopic measuring system (resolution of 1 μm and accuracy of ±8 μm). Channel depths were also measured at several points across the array using the Vickers CSS microscope. These depths varied from 252 to 280 μm, with the average depth being 273 μm. The difference in channel depth across a microchannel array can be attributed to non-uniformities in the plasma density of the deep reactive ion etch system and also the non-uniformity of the density of exposed silicon being etched.

The integrated sensors were calibrated using a reference T-type thermocouple to characterise the temperature-resistance relationship, which is shown in Fig. 4. The sensors positions are shown in Fig. 2a and had a typical sensitivity of 3.3 Ω/°C and an accuracy of ±0.5 °C using the present acquisition system. The thermal time constant associated with the nickel sensors was 1.6×10^{-4} s. Temperatures on the sensors and the inlet/outlet pressures were sampled at rates of 100 and 50 Hz. The advantage of using microfabricated temperature sensors in comparison to thermocouples is their much faster response time which resulted from the sensors being a 1 μm thick nickel film. The response time is practically instantaneous allowing high frequency sampling. In addition, integrated temperature sensors enable smaller thermal resistance between the sensors and channels. With thermocouples, there is inevitable gap between the heater and the silicon heat sink. An integrated heater provides a lower thermal resistance between the heater and the channels than a discrete heater allowing smaller heat losses, and hence better accuracy.

The test module inlet temperature was maintained within ±1 °C with the heater on the back side of the device being DC powered with a 1% uncertainty according to the manufacturer specifications. Visualisation of boiling within the channels was undertaken using a high speed camera (NanoSense MkIII), mounted on a microscope with a 5× magnification objective and axial illumination. The camera had a maximum frame rate of 1000 fps at full resolution of 1280 × 1024 pixels.

3. Results and discussion

3.1. Flow stability maps

In the present study, two types of two-phase flow boiling instabilities were identified for the heat sink consisting of 40 parallel rectangular microchannels. These were high amplitude/low frequency (HALF) and low amplitude/high frequency instabilities (LAHF) and were classified for the two inlet water temperatures of 25 and 71 °C. The results are presented using flow stability maps in terms of heat flux and mass flux with the criterion of classification being the frequency of the pressure drop oscillations. The pressure drop oscillations include the effects of all microchannels and give a representative fluctuation frequency for the system. It was found that frequencies typical of HALF type instabilities were in the range of 0.9–2.88 Hz. Frequencies typical of LAHF instabilities were in the range of 23–25 Hz, these latter are superimposed over a broad range of lower frequencies. Experiments were carried out at four different heat fluxes (178, 267, 356 and 445 kW/m^2) and two inlet subcooling conditions (25 and 71 °C). Fig. 5 shows

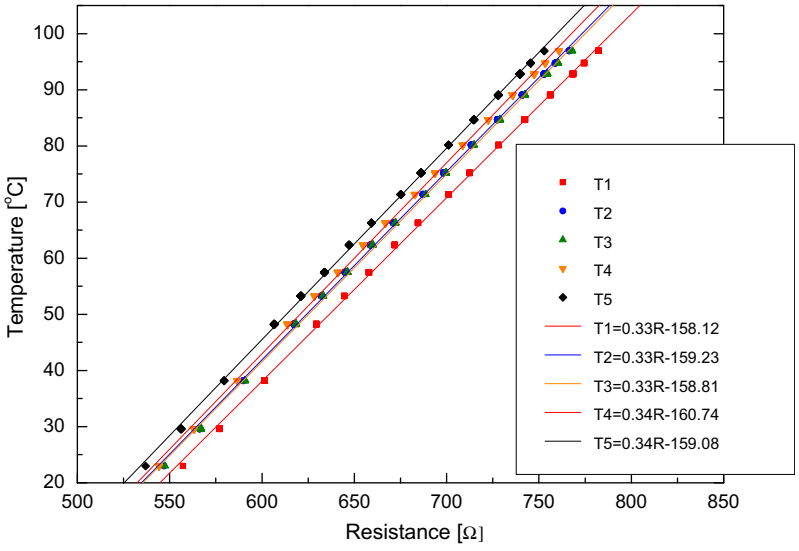

Fig. 4. Temperature calibration curves.

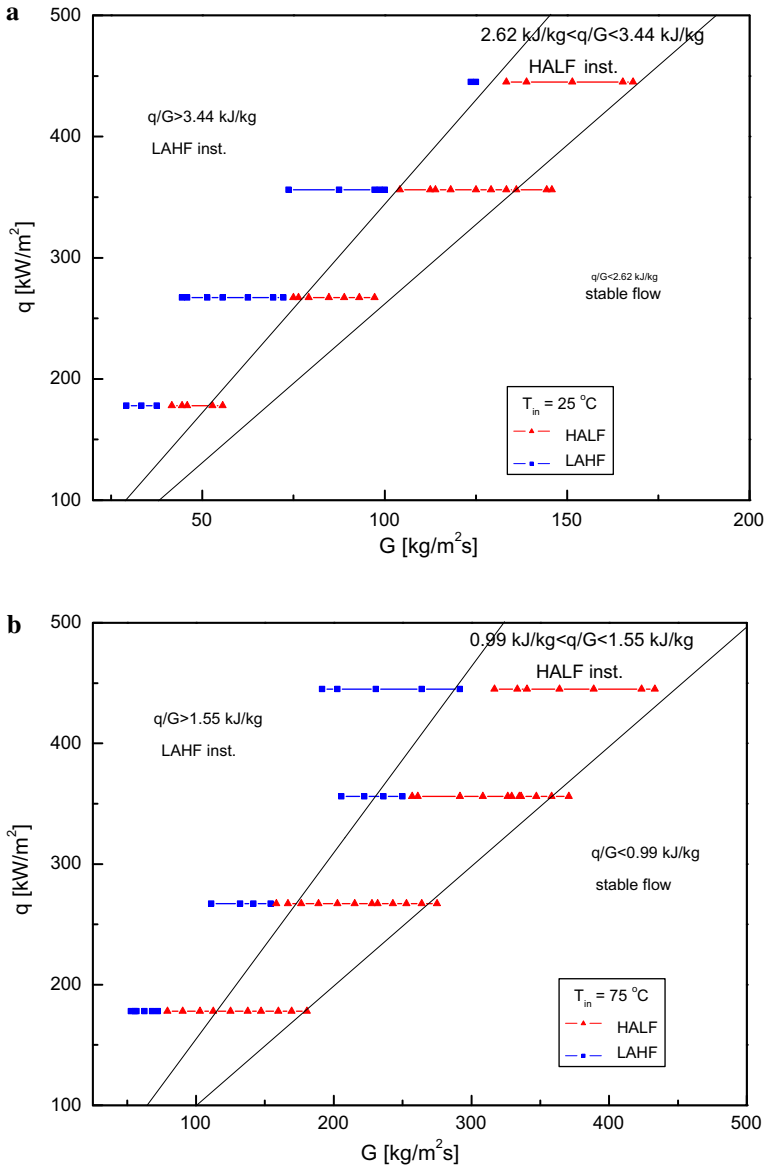

Fig. 5. Flow stability maps in parallel microchannels with hydraulic diameter of 194 μm for two different water inlet temperatures: (a) 25 °C and (b) 71 °C.

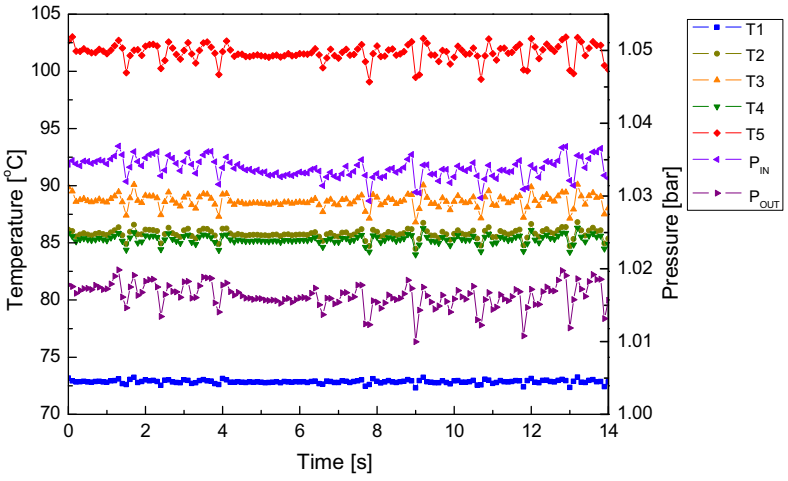

Fig. 6. Temporal variation of the sensor temperatures and the inlet/outlet pressures in stable flow regime with incipient boiling (q = 198.6 kW/m^2, G = 208 kg/m^2 s and T_{in} = 71 °C).

experimentally obtained flow stability maps in terms of heat flux and mass flux for two different inlet water temperatures. The two inclined straight lines divide the flow stability map into stable flow, unstable flow boiling with HALF instabilities and unstable flow boiling with LAHF instabilities.

The stable flow regime (q/G < 2.62 kJ/kg for T_{in} = 25 °C and q/G < 0.99 kJ/kg for T_{in} = 71 °C) includes single-phase flow and incipient flow boiling when isolated bubbles grow inside microchannels which are then flushed downstream by the bulk flow. Simultaneously performed measurements of inlet/outlet pressures and sensor temperatures for the case of stable flow regime with incipient boiling are presented in Fig 6. Fluctuations of the inlet/outlet pressure and the sensor's temperature are negligibly small in comparison to those found for unstable flow.

The slopes of the lines in the flow stability maps are defined by the ratio between heat flux and mass flux and it depends on the inlet water temperature. This implies that the flow stability depends on the q/G ratio as well as inlet subcooling condition. However, the experimental results show that boiling leads to very asymmetrical flow distribution within the 40 microchannels. This results in the simultaneous existence of different flow regimes inside microchannels along the transverse direction. Fig. 7a shows an image of bubbly flow pattern for a heat flux of 356 kW/m^2, a mass flux of 222.2 kg/m^2 s and inlet water temperature of 71 °C inside microchannels located above the sensor $T2$. Bubbles grew inside the microchannels, which are then carried downstream by the bulk flow. Fig. 7b shows an image of simultaneous transient annular flow inside the microchannels located above the sensor $T4$, at the same conditions of heat flux, mass flux and inlet water temperature (356 kW/m^2, 222.2 kg/m^2 s and 71 °C). Fig. 8a shows small fluctuations of the temperature $T2$, while appreciable fluctuations of the temperature $T4$ and the pressure drop. Frequency analysis of the pressure drop shown in Fig. 8b indicates LAHF type of instabilities. The pressure drop fluctuations inside the microchannels with transient annular flow dominate the pressure drop fluctuations due to bubbly flow.

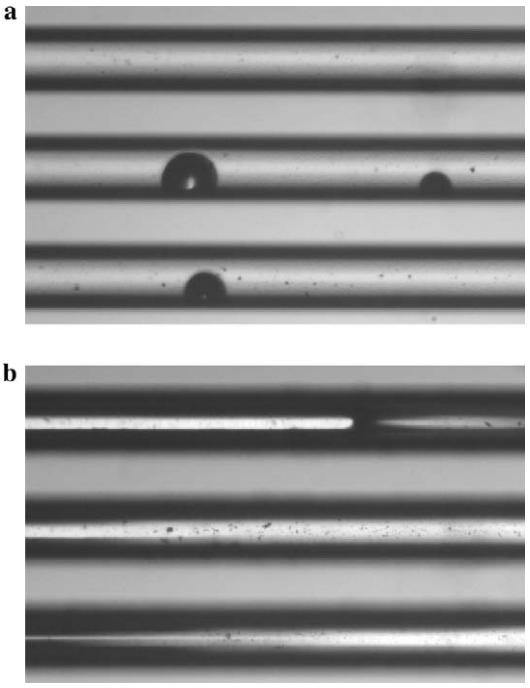

Fig. 7. (a) Image of bubbly flow pattern inside the microchannels located above the sensor $T2$ and (b) image of transient annular flow existed simultaneously inside the microchannels located above the sensor $T4$, q = 356 kW/m^2, G = 222.2 kg/m^2 s and T_{in} = 71 °C.

In the present investigation when the pressure was set to atmospheric, the boiling flow stability inside the heat sink was found to depend on the heat flux to mass flux ratio, inlet temperature and flow distribution within microchannels. Asymmetrical flow distribution within microchannels during flow boiling under constant heat flux might lead to the occurrence of LAHF instabilities at higher value of mass flux than is the case with uniform flow distribution within microchannels under the same heat flux. There are several possible reasons for the asymmetrical flow distribution during flow boiling inside the present heat sink with microchannels such as the shape and geometry of the inlet/outlet manifolds, the position of the inlet/outlet holes and uneven depth of the microchannels.

3.2. High amplitude low frequency (HALF) instabilities

Instabilities occur after the incipience of boiling inside the 194 μm hydraulic diameter channels, when increasing heat flux at a constant mass flux or decreasing mass flux with a constant heat flux. HALF instabilities existed for q/G ranging between 2.62 and 3.44 kJ/kg at inlet water temperature of 25 °C and q/G values from 0.99 to 1.55 kJ/kg with an inlet water temperature of 71 °C. Fig. 9 shows pressure and temperature oscillations simultaneously recorded at a 50 Hz sampling rate for a constant mass flow rate of 15 g/min (G = 208 kg/m^2 s), a heat flux of 209.6 kW/m^2 (q/G = 1.01 kJ/kg) and an inlet water temperature of 71 °C. The outlet temperature measured with a thermocouple oscillated between 96.4 and 101.4 °C with a mean value of 99.8 °C. The temperature on sensor $T1$, located at the inlet of microchannels region, oscillated with small amplitudes, while other signals oscillated with appreciable amplitudes. Fig. 10 presents the temperature fluctuations recorded for a constant mass flux of 208 kg/m^2 s, inlet water temperature of 71 °C and a range of heat fluxes. As the heat flux increases, the amplitude of temperature oscillations T1 increases as boiling propagates towards the inlet of microchannels. The amplitude of the temperature recorded on sensors $T5$, located at the outlet of microchannels region, decreases and the signal loses its sinusoidal shape, which was observed at q = 209.6 kW/m^2 and q = 219.6 kW/m^2. Differences between the temperatures $T2$, $T3$ and $T4$, located across the microchannels area, become more pronounced when increasing heat flux. This implies that boiling propagation towards the microchannels inlet leads to asymmetrical flow distribution within the microchannels.

The temporal behaviour of the inlet/outlet pressures and the corresponding pressure drop is shown in Fig. 11a for different heat fluxes and constant mass flux of 208 kg/m^2 s. The pressure drop oscillations and the inlet/outlet pressure oscillations are not in phase, implying that the inlet and the outlet pressure oscillations are also not in phase. The outlet pressure reaches the maximum earlier than the inlet pressure as the reverse vapour propagates from the microchannels outlet towards inlet during one cycle of HALF oscillations. Fast Fourier transform (FFT) analysis was performed on pressure drop data in order to obtain the frequency distribution for different heat fluxes and is shown in Fig 11b. This analysis shows that the frequency of oscillation decreases with increasing heat flux with constant mass flux. The frequencies of the pressure drop oscillations obtained from the experiments with constant heat flux and varied mass flux are presented in Table 1 for two different inlet water temperatures. The mass flux was varied from high to low values and the frequencies in Table 1 are presented for the beginning and the end of the HALF instabilities for each of the four heat fluxes. The pressure drop oscillation frequencies were found to decrease when mass flux decreases at a constant heat flux.

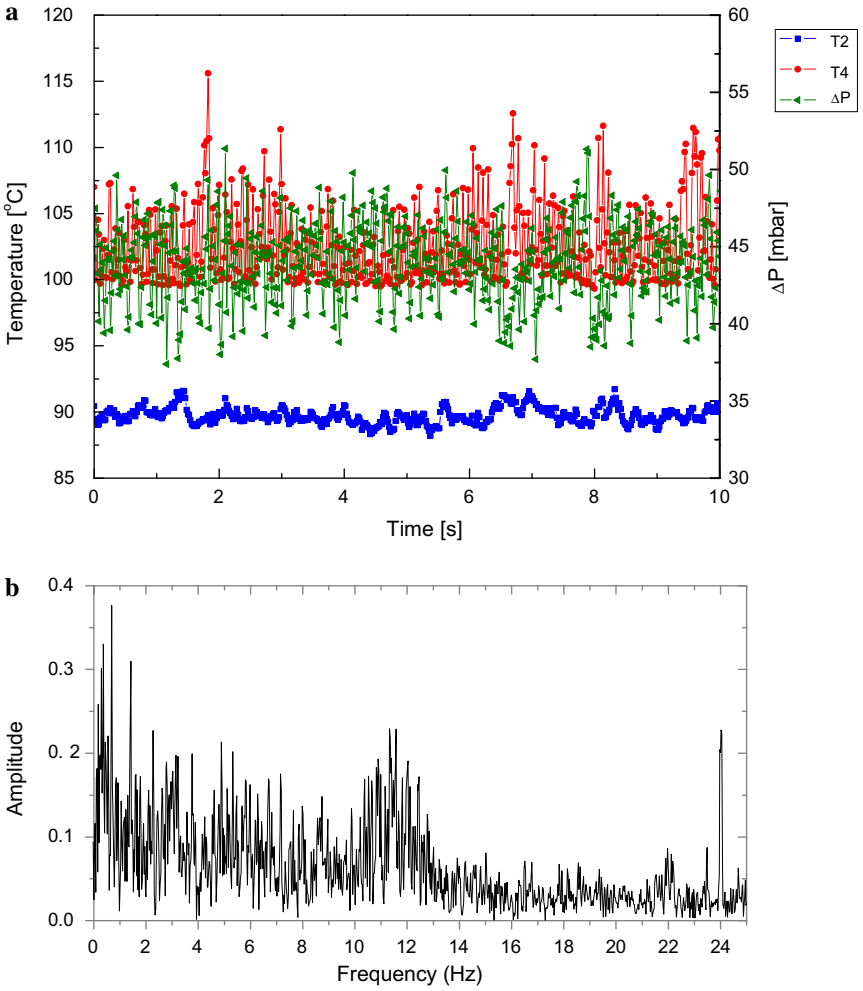

Fig. 8. (a) Measurements of temperatures $T2$, $T4$ and pressure drop for non-uniform flow distribution within parallel microchannels $q = 356$ kW/m^2, $G = 222.2$ kg/m^2 s and $T_{in} = 71$ °C and (b) pressure drop frequency analysis.

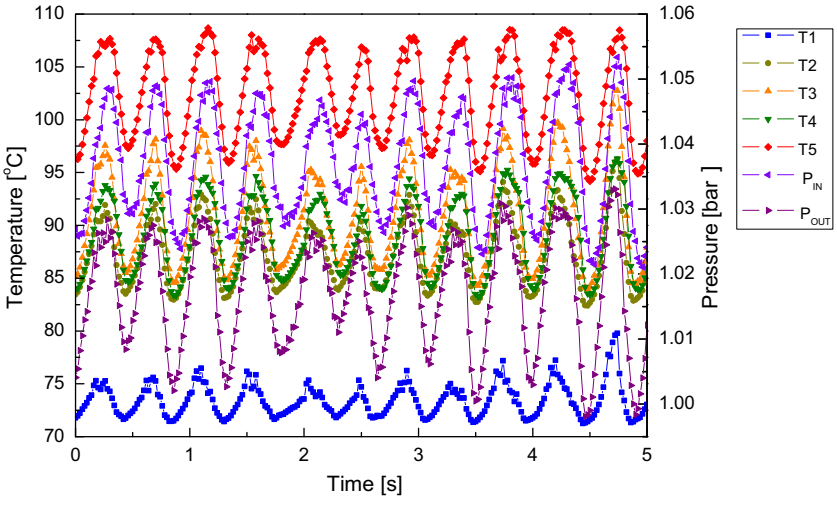

Fig. 9. Sensor temperature and inlet/outlet pressure oscillations in unstable flow boiling regime with HALF instabilities ($q = 209.6$ kW/m^2, $G = 208$ kg/m^2 s, and $T_{in} = 71$ °C).

The observed frequencies (periods) are different from those reported by Wang et al. (2007). These authors observed periods ranging from approximately 2.5–9.5 s (0.1–0.4 Hz), while we observed frequencies ranging between 0.9 and 2.88 Hz for the case of high amplitude/low frequency oscillations. It is suggested that these observed differences are probably due to the fact that during the experiments conducted by Wang et al. the mass flux fluctuated while in our experiments this was kept constant. In an earlier work

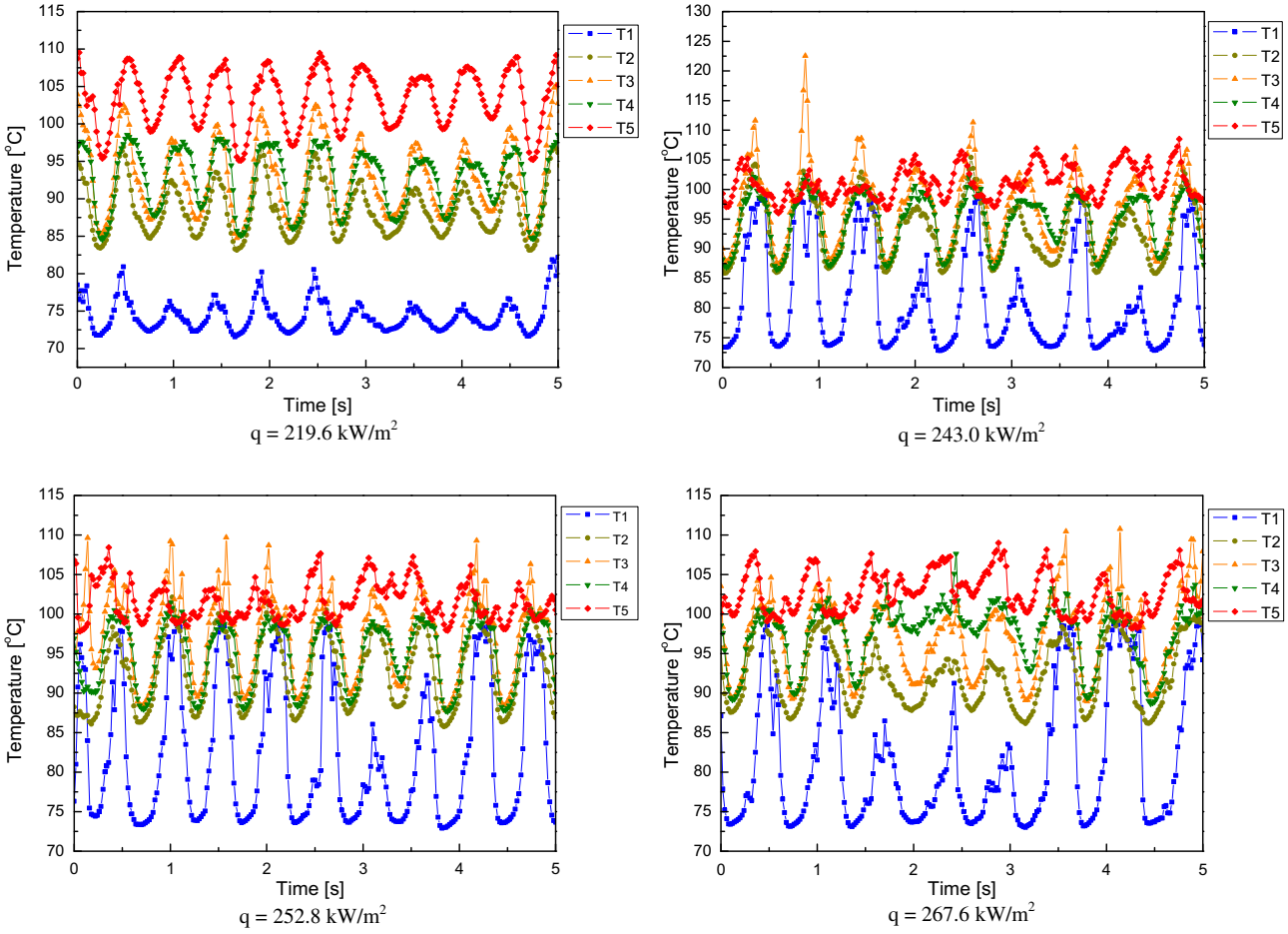

Fig. 10. Sensor temperature fluctuations in unstable flow regime with HALF instabilities for a mass flux of 208 kg/m^2 s, inlet water temperature of 71 °C and a range of heat fluxes.

Wu and Cheng (2004) used the same microchannels and experimental test loop as in the study of Wang et al. (2007) and reported much longer oscillation periods ranging from 15.4 to 202 s for average values of mass flux from 112 to 146 kg/m^2 s with a heat flux between 135 and 226 kW/m^2. The authors used compressed nitrogen gas to move the water from the pressure tank to the test section with microchannels and reported that when boiling occurred the pressure drop across the test section suddenly increased due to generation of vapour bubbles. Because pressure drop and mass flux are coupled, this increase in pressure drop caused a decrease in mass flux, which in turn caused the pressure drop to decrease. As a result, pressure and mass flux oscillations occurred. The period of increase or a decrease of incoming mass flux may be a reason for the long-period oscillations in temperatures and pressures, reported by the authors.

Similar frequency values and trends to those observed for HALF instabilities in our experiments have been reported by Hetsroni et al. (2006) in their experimental study of flow boiling instabilities in parallel microchannels at low vapour quality. It is interesting to note that the authors used a pump to deliver cooling water into the test section at constant flow rate and reported the frequencies of the pressure drop and temperature oscillations ranged between 1.6 and 2.8 Hz. In addition, they found that periods of oscillation increased with increasing power. However, they reported only one mode of instability, probably because of using lower values of the heat fluxes for a similar condition of the mass flux used in our experiments. The authors reported an increase in amplitudes of temperatures and pressures with increasing heat flux. We observed that amplitudes increased first then decreased as the system passed from the high amplitude/low frequency towards the low amplitude/high frequency instabilities with heat flux increasing under constant mass flux, or mass flux decreasing under constant heat flux.

Temperature, inlet/outlet pressure and pressure drop fluctuations during the HALF instabilities indicate reverse vapour flow inside the channels. Simultaneous video visualisation confirmed that these fluctuations are caused by the flow alternating between liquid, two-phase and vapour flow. Similar observation have been reported by Hetsroni et al. (2005, 2006) and Wang et al. (2007). Fig. 12 shows image sequences from a recording captured using a high speed camera at a frame rate of 500 fps. These images are related to the HALF instabilities for a heat flux of 243.0 kW/m^2, mass flux of 208 kg/m^2 s and an inlet water temperature of 71 °C. The arrow in the first image shows the direction of the water flow and the circle marks the nucleation site. After the microchannel with the marked nucleation site is filled with water (t = 0 ms), the bubble grows (t = 82 ms) and occupies the entire channel diameter. Further axial growth causes bubbles to expand (t = 150 ms) forming a transient wispy annular flow as can be observed in the image when t = 180 ms. The vapour generated after the bubble bursts expands both downstream, increasing outlet pressure, and upstream, pushing the liquid front back leading to reverse flow and an increase of inlet pressure. The image captured at t = 212 ms shows the onset of a temporary "dry out" period inside the channel. This temporary "dry out" period occurs due to thin liquid film evaporation in the transient wispy annular flow.

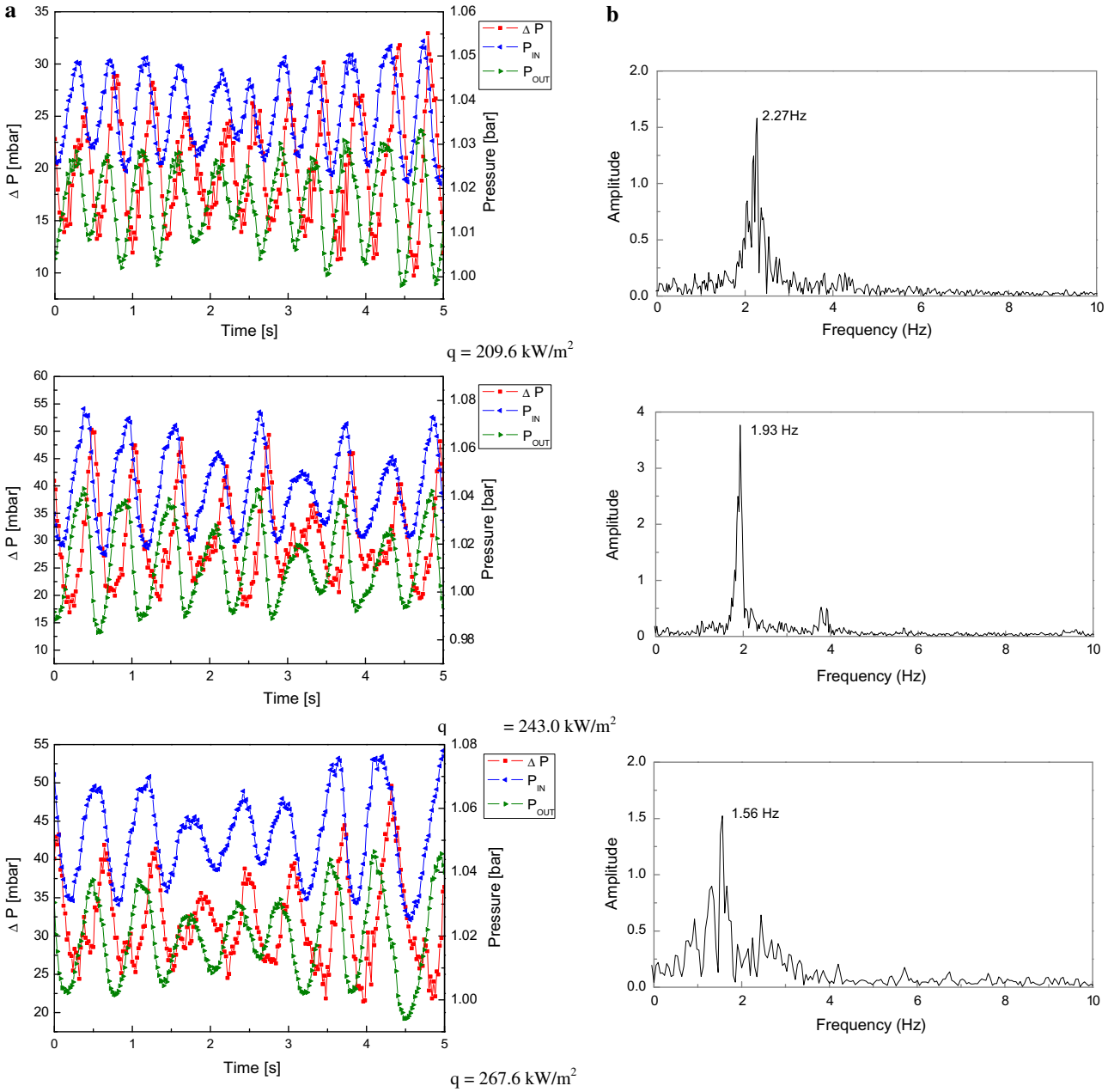

Fig. 11. (a) Pressure drop fluctuations in unstable flow regime with HALF instabilities for a mass flux of 208 kg/m^2 s, inlet water temperature of 71 °C and a range of heat fluxes and (b) pressure drop frequency analysis.

Table 1
The frequencies of the pressure drop oscillations obtained from the experiments with constant heat flux and varied mass flux for two inlet water temperatures of 25 and 71 °C.

Heat flux q (kW/m^2)	T_{in} = 71 °C		T_{in} = 25 °C	
	Mass flux G (kg/m^2 s)	Frequency f (Hz)	Mass flux G (kg/m^2 s)	Frequency f (Hz)
178	72.2	1.07	41.7	1.95
	180.6	2.00	55.6	2.64
267	158.3	1.10	75.0	1.19
	275.0	2.20	97.2	2.59
356	256.9	2.17	104.2	1.32
	370.8	2.34	145.8	2.71
445	316.7	2.10	133.3	0.90
	433.3	2.88	168.1	2.22

The "dry out" period was found to increase with increasing heat flux for the HALF instabilities. This leads to a rise in the period for one oscillation, and therefore lower frequencies. The incoming subcooled liquid condenses vapour and a new cycle starts with

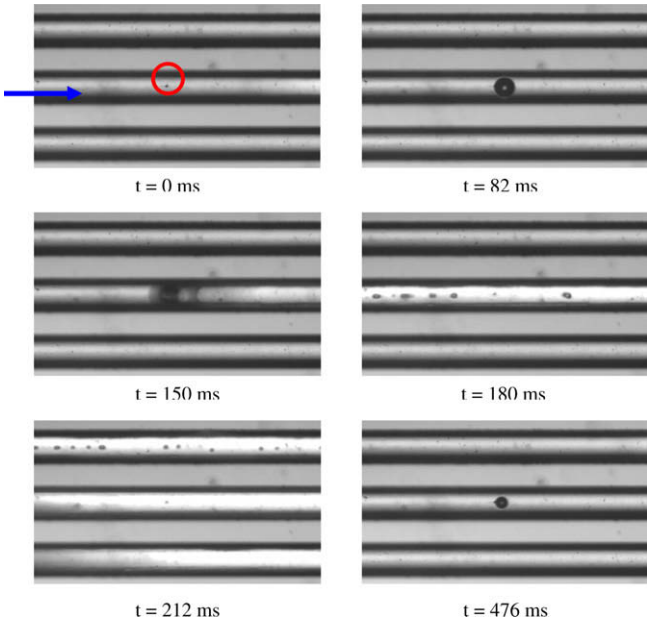

Fig. 12. Image sequences of flow boiling with HALF instabilities inside the parallel microchannels with hydraulic diameter of 194 μm (q = 243.0 kW/m^2, G = 208 kg/m^2 s and T_{in} 71 °C).

bubble nucleation when the subcooled liquid refills the channel downstream from the nucleation site (t = 476 ms). It was observed that alternations between liquid, two-phase and vapour flow in adjacent channels are not in phase (e.g. Fig. 12, t = 180 ms, wispy annular flow present in the middle channel while two adjacent channels are filled with liquid water). However, it was clearly observed that there were short periods when the liquid phase exists inside all microchannels and this was captured using a high speed camera using a 2300 μm diameter field of view, covering about nine channels. This period corresponds to minima in the temperature and the pressure drop measurements during the HALF instabilities. The time elapsed between two successive "refills" measured from the video is 0.476 s for a heat flux of 243.0 kW/m^2, a mass flux of 208 kg/m^2 s and an inlet temperature of 71 °C. The average time between two successive pressure drop minima measured from a simultaneously acquired experimental data set (Fig. 11a, q = 243.0 kW/m^2) is 0.5 s and it is in good agreement with the time measured from the video. At a lower heat flux of 209.6 kW/cm^2 bubbles nucleation and growth was observed only close to the microchannels exit. With an increase of the heat flux, boiling propagates towards the microchannels inlet causing vapour expansion inside the inlet manifold. Fig. 13 shows backward expansion of the vapour jet into the inlet manifold at a heat flux of 243.0 kW/m^2, mass flux of 208 kg/m^2 s and inlet water temperature of 71 °C. The process of alternation between liquid, two-phase and vapour flow repeats in cycles when both the heat flux and water flow rates are constant inside the channels.

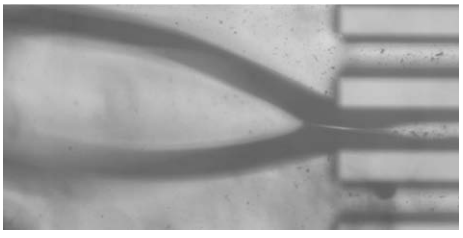

Fig. 13. Image sequence of flow boiling with HALF instabilities captured using high speed camera at frame rate of 500 fps. The vapour jet from the microchannel expands inside the inlet manifold of the heat sink.

3.3. Low amplitude high frequency (LAHF) instabilities

This type of two-phase flow instabilities inside microchannels was observed after HALF instabilities, when increasing the heat flux at a constant mass flux or decreasing the mass flux at a constant heat flux. LAHF instabilities existed for the case of q/G > 3.44 kJ/kg at inlet water temperature of 25 °C and q/G > 1.55 kJ/kg at inlet water temperature of 71 °C. Fig. 14a shows temperature sensor measurements for LAHF type two-phase instabilities inside the microchannels for two different heat fluxes: 321.7 and 400.4 kW/m^2, constant mass flux of 208 kg/m^2 s and inlet water temperature of 71 °C. Although, the inlet and outlet pressures oscillated with smaller amplitudes than those found for HALF instabilities, appreciable fluctuations of temperatures, especially those measured by sensor T1 located at channels inlet, were observed. Wang et al. (2007) reported nearly constant inlet and outlet temperatures of water as well as wall temperatures for the case of "short-period" oscillation. They reported the thermocouples used for temperature measurements had a response time of 0.1 s, which was too slow to measure any high frequencies associated with "short-period" oscillations.

We observed temperature oscillations with irregular amplitudes and frequencies higher than those found for the HALF type of instabilities. Temperature measured by sensor T1, located at the inlet of microchannels region, oscillated with high amplitudes, while other signals exhibited smaller amplitudes. With an increase of the heat flux, the amplitude of temperature T1 decrease as the period of the liquid phase becomes shorter inside the microchannels. The increase of the heat flux leads to a rise in magnitudes of temperatures T3, T4 and T5 (Fig. 14a, q = 400.4 kW/m^2). Significant difference between temperatures T2 and T4 indicates asymmetrical flow distributions within the microchannels. Temporal fluctuations of inlet/outlet pressure and the corresponding pressure drop simultaneously measured with the temperatures in Fig. 14a are presented in Fig. 14b. Inlet/outlet pressure and pressure drop oscillate with high frequency and irregular low amplitudes. The magnitudes of the inlet/outlet pressure and the pressure drop oscillations increase with increasing heat flux. FFT analysis was performed on the pressure drop data and the results are presented in Fig. 14c. Frequency analysis shows a wide range of low frequencies and clear peaks around 24 Hz. This is characteristic of this type of instabilities where frequencies in the range of 23–25 Hz are superimposed on a broad range of lower frequencies. It is interesting to note that Wang et al. (2007) reported a similar value of 22 Hz for the inlet pressure oscillation under a boiling regime with "short-period" oscillation. The authors concluded that the frequency of pressure fluctuations was independent of the mass flux. This may be a reason to why we observed similar frequencies for the case of LAHF as Wang et al. (2007) reported for "short-period" oscillation, although significantly different frequencies were observed for the case of HALF oscillations compared with those observed by Wang et al. (2007) for "long-period" oscillations. The latter is due to the fact that the frequency of oscillations for HALF instabilities ("long-period" oscillations reported by Wang et al. (2007)) is strongly dependent on the mass flux. Wang et al. (2007) reported frequencies of 32 Hz at a heat flux of 740.7 kW/m^2. We have not observed such high frequencies even at a data acquisition sampling rate of 100 Hz. A possible reason is that we used smaller heat fluxes (the maximum heat flux used in our experiments was 590.4 kW/m^2).

Simultaneous visualisation of boiling inside the channels indicates that these fluctuations are caused by alternation between liquid, two-phase and vapour flow. The liquid phase lasts for a

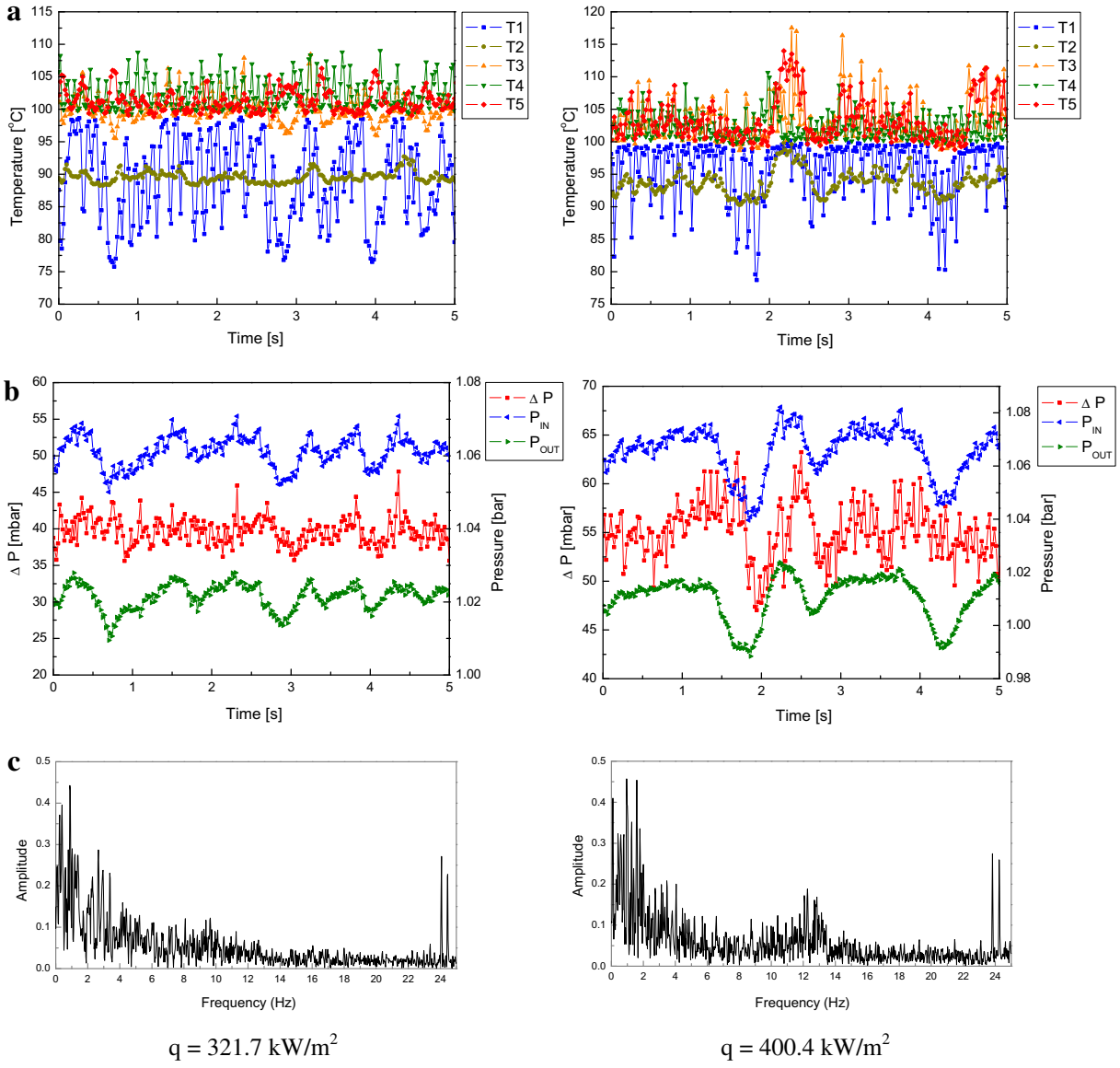

Fig. 14. Measurements recorded during the unstable flow with LAHF instabilities for a mass flux of 208 kg/m^2 s, an inlet temperature of 71 °C and two heat fluxes of 321.7 kW/m^2 and 400.4 kW/m^2: (a) sensor temperature measurements, (b) inlet/outlet pressure and pressure drop measurements for two heat fluxes and (c) frequency analysis of the pressure drop.

shorter period than in the case of HALF instabilities, turning into droplets and a liquid film, which quickly evaporate. Bubbles nucleation and growth observed inside the bulk flow lasts for a much shorter period than is the case for high amplitude/low frequency instabilities. Fig. 15 shows image sequences captured using the high speed camera at a frame rate of 500 fps. These images show bubble nucleation, growth and burst during the LAHF instabilities inside the microchannel with a nucleation site. The nucleation site is marked with the circle and the arrow shows the flow directions (Fig. 15 image t = 0 ms). It is clear from Fig. 15 that alternations in adjacent channels was not in phase (non-synchronous alternation within channels). The latter is consequence of the non-uniform distribution of cooling water within 40 channels. The bubble growth time is around 16 ms with the bubble bursting before occupying the entire channel diameter. The image at t = 16 ms shows transient annular flow formed after the bubble bursts inside the channel with the nucleation site. The thin liquid film of annular flow rapidly evaporates, causing a temporal "dry out" period inside the observed channel as shown in the image at t = 48 ms. The aver-

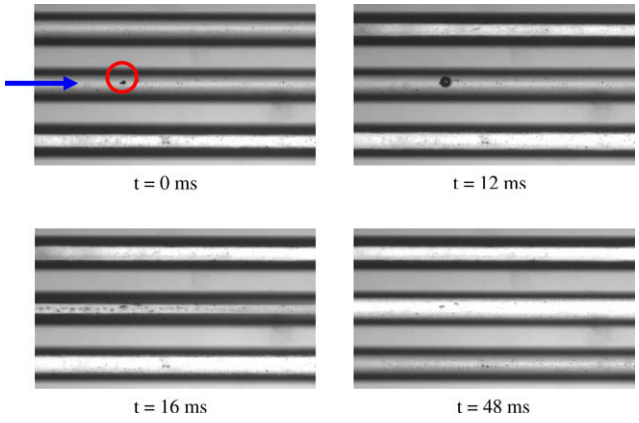

Fig. 15. Image sequences of flow boiling with LAHF instabilities inside the parallel microchannels with hydraulic diameter of 194 μm (q = 400.4 kW/m^2, G = 208 kg/m^2 s and T_{in} 71 °C).

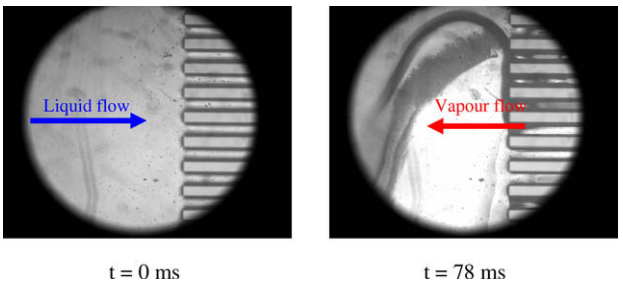

Fig. 16. Alternation inside the inlet manifold between the liquid flow (t = 0 ms) and the reverse vapour flow from microchannels (q = 356 kW/m^2, G = 222.2 kg/m^2 s, T_{in} = 71 °C).

age period between two successive "refills" measured from the video for the channel with the marked nucleation site is 96 ms. In general, the bubble growth time and the period between two successive "refills" are shorter than in the case of HALF oscillations. Hence, frequencies of LAHF oscillations are higher than those found for the HALF type of instabilities. A large amount of reverse vapour flow was observed inside the inlet manifold during the LAHF instabilities. Fig. 16 shows image sequences of the alternation between the incoming liquid flow (t = 0 ms) and the reverse vapour flow from the microchannels (t = 78 ms) for a heat flux of 356.0 kW/m^2, a mass flux of 222.2 kg/m^2 s (q/G = 1.60 kJ/kg) and an inlet temperature of 71 °C.

The LAHF type of instabilities was observed in the experiments with a constant heat flux when decreasing the mass flux for both of the water inlet temperatures used in the experiments (25 and 71 °C). The frequencies ranged between 23 and 24 Hz, superimposed over a broad range of lower frequencies.

3.4. Pressure drop characteristic and temperature analysis in microchannels

The determination of the relationship between pressure drop and flow rate (internal characteristic curve) is crucial in the investigation of the two-phase flow instabilities in microchannel heat sinks. A minimum in the curve is the necessary condition for the compressible volume instability and the excursive instabilities (Bergles and Kandlikar, 2005). Fig. 17 shows averaged values of the pressure drop as a function of mass flux curves in the microchannels obtained at different heat fluxes for two inlet water temperatures of 25 and 71 °C. There is a characteristic minimum for each curve corresponding to incipient flow boiling in the stable flow regime. A decrease of the mass flux or increase of the heat flux from the minimum point leads to a higher pressure drop due to

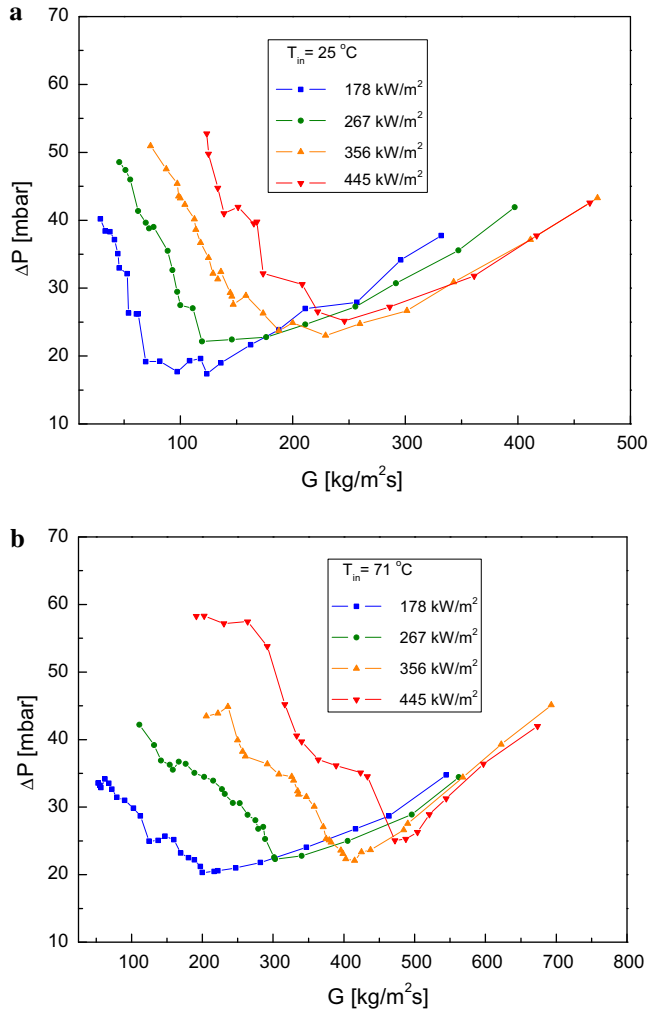

Fig. 17. Pressure drop characteristic of the heat sink with parallel microchannels with hydraulic diameter of 194 μm for the different heat fluxes with (a) T_{in} = 25 °C and (b) T_{in} = 71 °C.

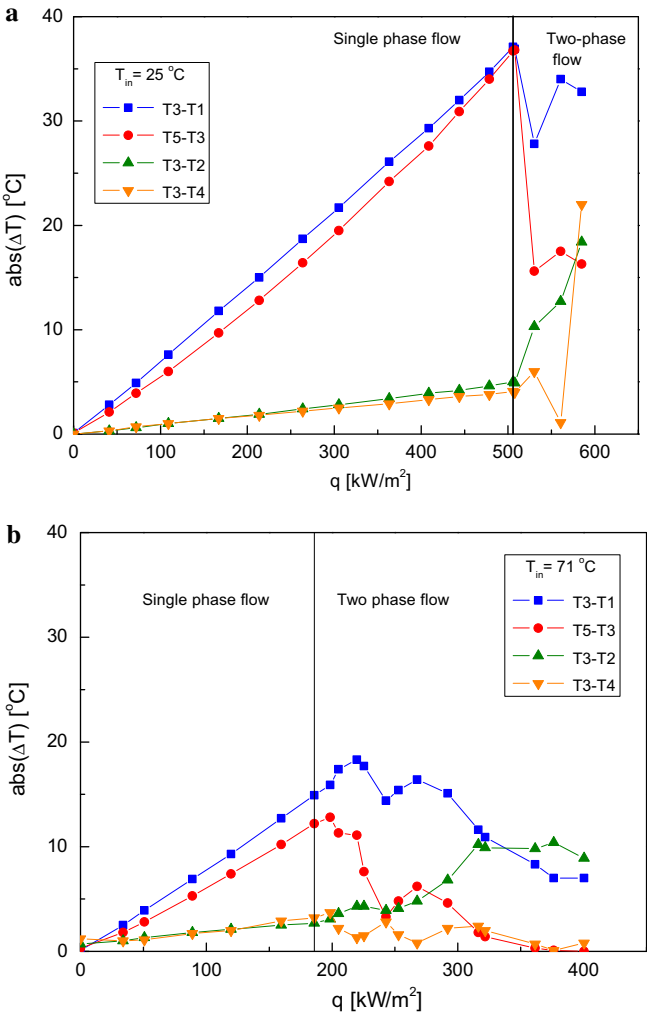

Fig. 18. Absolute differences between the average temperatures measured by the sensors vs. heat flux, G = 208 kg/m^2 s, T_{in} = 25 °C (a) and T_{in} = 71 °C (b).

vapour generation. The pressure drop characteristic curves exhibit high negative slope for the two-phase flow region indicating two-phase flow instabilities at the both inlet subcooling conditions (25 and 71 °C). High amplitude oscillations were observed for both the inlet and the outlet pressure. For comparison Wang et al. (2007) reported only appreciable fluctuations of the inlet pressure. The magnitude of the pressure drop oscillations (difference between maximum and minimum values of the pressure drop) depends on the q/G ratio and T_{in}. In the case of stable flow with incipient boiling the magnitude was found to be in the range of 5–10 mbar. Values of the magnitude for the HALF instabilities ranged from 25 mbar to 86 mbar. The maximum value of 85.4 mbar was found for T_{in} = 25 °C, mass flux of 208 kg/m^2 s and heat flux of 530.4 kW/m^2, while for the same mass flux and T_{in} = 71 °C the maximum magnitude of the pressure drop oscillation was 42.6 mbar for a heat flux of 243.0 kW/m^2. It was found that the magnitude of pressure drop oscillations for the HALF instabilities first increased and then decreased with heat flux increasing at a constant mass flux or with mass flux decreasing at a constant heat flux. Magnitudes for the LAHF instabilities ranged between 10 and 25 mbar. However, the occurrence of permanent local "dry out" zone observed at the low mass fluxes or the high heat fluxes might lead to a sudden rise in the pressure drop during the LAHF instabilities.

It has been pointed out that boiling inside microchannels leads to asymmetrical flow distribution and the simultaneous existence of different flow patterns inside microchannels along the transverse direction in the present experimental heat sink. A significant difference between temperatures measured on the sensors located in the transverse direction (sensors *T*2, *T*3 and *T*4) existed as a consequence of the asymmetrical flow distribution within the microchannels during flow boiling. Fig. 18 presents the temperature distribution along the flow stream direction and the transverse direction for the mass flux of 208 kg/m^2 s for two different inlet water temperatures (25 and 71 °C) and a range of heat fluxes. Fig. 18 shows absolute differences between the average temperatures measured by the sensors. In the single-phase flow regime the differences between the sensors located in the transverse direction *T*3–*T*2 and *T*3–*T*4 are very small, less then 1 °C, indicating uniform distribution for both inlet water temperatures. However, incipience of boiling inside the microchannels affects flow distribution causing an appreciable difference between the values of *T*3–*T*2 and *T*3–*T*4 (Fig. 18a and b). A significant difference exists for both inlet water temperatures indicating asymmetrical flow distribution. However, asymmetrical flow distribution is more transparent for the lower temperature of 25 °C. At the heat flux of 584.9 kW/m^2 and T_{in} = 25 °C the mean value of the T4 temperature measurement was 110.3 °C, while that for the *T*2 sensor was 69.9 °C. Asymmetrical flow distribution at a low inlet temperature of 25 °C caused a permanent local "dry out" zone inside the microchannels located above the sensor *T*4 before the occurrence of LAHF instabilities inside the microchannels. Fig. 19 shows temperature measurements when the "dry out" zone was observed inside the heat sink for q = 590.4 kW/m^2, G = 208 kg/m^2 s and T_{in} = 25 °C.

With boiling incipience inside the microchannels, differences between the average temperatures on the sensors located along the direction of the flow stream (*T*3–*T*1 and *T*5–*T*3) become smaller. This implies that boiling leads to a better temperature uniformity in the direction of the flow stream. High inlet temperature (75 °C) gives smaller sensors temperature differences and better temperature uniformity along the direction of the flow stream and the transverse direction, indicating better flow distribution than in the case of low inlet water temperature (25 °C).

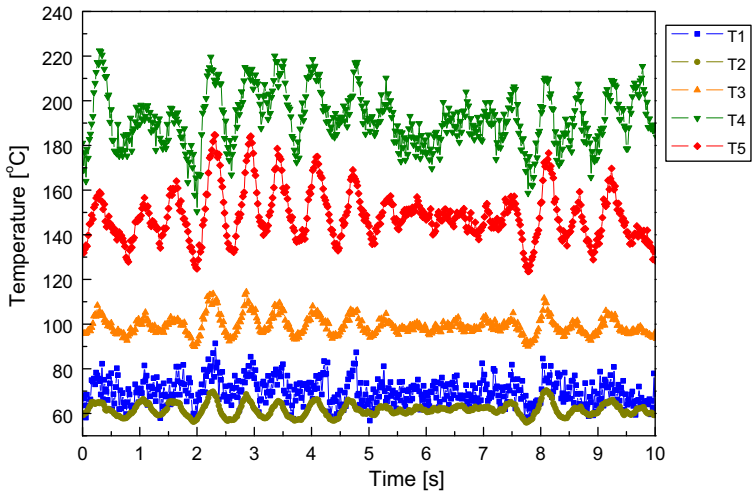

Fig. 19. Temperature measurements for q = 590.4 kW/m^2, G = 208 kg/m^2 s and T_{in} = 25 °C. "Dray out" zone existed inside the channels above the sensors *T*4.

Table 2
Maximum magnitudes of temperatures *T*1, *T*2 and *T*3 found for the different heat fluxes and inlet water temperatures.

Heat flux q (kW/m^2)	T_{in} (°C)	Magnitude $T1_{max}$–$T1_{min}$ (°C)	Magnitude $T3_{max}$–$T3_{min}$ (°C)	Magnitude $T5_{max}$–$T5_{min}$ (°C)
178.0	25	58.2	45.2	38.7
178.0	71	33.8	53.7	37.9
267.0	25	58.6	55.6	59.5
267.0	71	28.4	28.7	22.7
356.0	25	61.5	49.6	35.9
356.0	71	27.3	15.9	22.5
445.0	25	60.5	69.0	43.8
445.0	71	27.8	61.2	41.2

It was found that the inlet temperature affects the magnitude of the temperature oscillations during two-phase flow instabilities. Table 2 presents the magnitudes (differences between maximum and minimum temperature from one data set) of temperature measurements on sensors $T1$, $T3$ and $T5$ for inlet water temperature of 25 °C and 71 °C with four different heat fluxes. Each value of magnitude in Table 2 is the maximum value measured for a range of mass fluxes at a particular heat flux and inlet water temperature. In general, lower inlet water temperature leads to higher magnitudes of temperature oscillations (the only exception is the magnitude of the temperature $T3$ for a heat flux of 178.0 kW/m^2 where the magnitude is higher for a higher temperature). Alternation between the incoming liquid at high subcooling condition and reverse flow of vapour causes oscillations of the temperature with significant magnitudes, especially those measured on sensors $T1$ located at the microchannels inlet and $T3$ located in the middle of the heat sink.

4. Conclusion

In this study, simultaneous measurements and visualisation experiments have been performed in order to examine two-phase flow instabilities in a microchannels based heat sink with 40 parallel rectangular channels having hydraulic diameter of 194 μm, using water at two different inlet temperatures: 25 and 71 °C. In the light of these experiments, two types of two-phase instabilities were identified: one with high amplitude/low frequency oscillations (HALF) and the other with low amplitude/high frequency oscillations (LAHF). The criterion of classification was the frequency and amplitude of the pressure drop oscillations. It was found that the flow regime and type of two-phase flow instabilities depended on the q/G ratio and inlet subcooling condition. However, the experimental results show that two-phase instabilities lead to very asymmetrical flow distribution within the 40 microchannels and result in the simultaneous existence of different flow regimes inside microchannels along the transverse direction.

HALF instabilities existed for q/G range from 2.62 to 3.44 kJ/kg at inlet water temperature of 25 °C and q/G range from 0.99 to 1.55 kJ/kg at inlet water temperature of 71 °C. It was found that frequencies of the pressure drop oscillations typical for HALF instabilities were in the range of 0–3 Hz. The frequency of HALF oscillations decreased with increasing heat flux or decreasing mass flow rate. The inlet/outlet pressure oscillations are not in phase as the outlet pressure reaches the maximum earlier than the inlet pressure due to reverse vapour propagation from the microchannels outlet towards inlet during one cycle of HALF oscillations. Simultaneous visualisation and measurement indicate that pressure and temperature fluctuations, characteristic of HALF instabilities are caused by alternation between liquid, two-phase and vapour flow (temporary "dry out" period). The bubble grows occupying the entire channels diameter and its growth time is longer than in the case of LAHF instabilities. The magnitude of pressure drop oscillations (difference between maximum and minimum values of the pressure drop) ranged between 25 and 86 mbar. It was found that the magnitudes of pressure drop oscillations for the HALF instabilities first increased and then decreased with the heat flux increasing at a constant mass flux or with mass flux decreasing at a constant heat flux.

LAHF instabilities exist for the cases when $q/G > 3.44$ kJ/kg at an inlet water temperature of 25 °C and $q/G > 1.55$ kJ/kg at inlet water temperature of 71 °C. Frequencies typical for LAHF instabilities were in the range of 23–25 Hz, superimposed over a broad range of lower frequencies. The magnitudes of pressure drop measurements for the LAHF instabilities ranged between 10 and 25 mbar. The occurrence of a permanent local "dry out" zone might lead to sudden rise in the pressure drop during the LAHF instabilities. High speed camera imaging shows that bubble growth time and period between two successive "refills" of the microchannels are shorter than in the case of HALF oscillations. This leads to existence of the higher oscillations frequencies during LAHF instabilities than those found for the HALF instabilities.

It was found that inlet water temperature affects the magnitudes of the temperature oscillations during two-phase flow instabilities. Lower inlet water temperature leads to higher magnitudes of temperature oscillations. Higher inlet temperature gives better temperature uniformity along the direction of the flow stream and the transverse direction, indicating better flow distribution than in case of lower inlet water temperature.

Acknowledgements

This research was supported by the UK Engineering and Physical Sciences Research Council through Grant EP/D500109/1. The authors in the Institute of Integrated Systems would also like to acknowledge the support from the Scottish Funding Council for the Joint Research Institute of Integrated Systems with the Heriot-Watt University and UKATC which is a part of the Edinburgh Research Partnership in Engineering and Mathematics (ERPem).

References

Bergles, A.E., Kandlikar, S.G., 2005. On the nature of critical heat flux in microchannels. Journal of Heat Transfer 127, 101–107.
Hetsroni, G., Mosyak, A., Pogrebnyak, E., Segal, Z., 2005. Explosive boiling of water in parallel micro-channels. International Journal of Multiphase Flow 31, 371–392.
Hetsroni, G., Mosyak, A., Pogrebnyak, E., Segal, Z., 2006. Periodic boiling in parallel micro-channels at low vapor quality. International Journal of Multiphase Flow 32, 1141–1159.
Hetsroni, G., Mosyak, A., Segal, Z., Pogrebnyak, E., 2003. Two-phase flow patterns in parallel micro-channels. International Journal of Multiphase Flow 29, 341–360.
Hetsroni, G., Mosyak, A., Segal, Z., Ziskind, G., 2002. A uniform temperature heat sink for cooling of electronic devices. International Journal of Heat and Mass Transfer 45, 3275–3286.
Kandlikar, S.G., Kuan, W.K., Willistein, D.A., Borrelli, J., 2006. Stabilization of flow boiling in microchannels using pressure drop elements and fabricated nucleation sites. Journal of Heat Transfer 128, 389–396.
Kosar, A., Kuo, C.-J., Peles, Y., 2006. Suppression of boiling flow oscillations in parallel microchannels by inlet restrictors. Journal of Heat Transfer 128, 251.
Kuo, C.J., Peles, Y., 2009. Pressure effects on flow boiling instabilities in parallel microchannels. International Journal of Heat and Mass Transfer 52, 271–280.
Lin, S., Sefiane, K., Christy, J.R.E., 2002. Prospects of confined flow boiling in thermal management of microsystems. Applied Thermal Engineering 22, 825–837.
Liu, D., Lee, P.-S., Garimella, S.V., 2005. Prediction of the onset of nucleate boiling in microchannel flow. International Journal of Heat and Mass Transfer 48, 5134–5149.
Qu, W., Mudawar, I., 2003. Measurement and prediction of pressure drop in two-phase micro-channel heat sinks. International Journal of Heat and Mass Transfer 46, 2737–2753.
Wang, G., Cheng, P., Bergles, A.E., 2008. Effects of inlet/outlet configurations on flow boiling instability in parallel microchannels. International Journal of Heat and Mass Transfer 51, 2267–2281.
Wang, G., Cheng, P., Wu, H., 2007. Unstable and stable flow boiling in parallel microchannels and in a single microchannel. International Journal of Heat and Mass Transfer 50, 4297–4310.
Wu, H.Y., Cheng, P., 2003a. Liquid/two-phase/vapor alternating flow during boiling in microchannels at high heat flux. International Communications in Heat and Mass Transfer 30, 295–302.
Wu, H.Y., Cheng, P., 2003b. Visualization and measurements of periodic boiling in silicon microchannels. International Journal of Heat and Mass Transfer 46, 2603–2614.
Wu, H.Y., Cheng, P., 2004. Boiling instability in parallel silicon microchannels at different heat flux. International Journal of Heat and Mass Transfer 47, 3631–3641.
Zhang, L., Wang, E.N., Goodson, K.E., Kenny, T.W., 2005. Phase change phenomena in silicon microchannels. International Journal of Heat and Mass Transfer 48, 1572–1582.